nature human behaviour

ARTICLES

https://doi.org/10.1038/s41562-020-01027-y

Check for updates

Genetic underpinnings of risky behaviour relate to altered neuroanatomy

Gökhan Aydogan[1], Remi Daviet[2], Richard Karlsson Linnér[3], Todd A. Hare[1], Joseph W. Kable[2,4], Henry R. Kranzler[5,6], Reagan R. Wetherill[5], Christian C. Ruff[1], Philipp D. Koellinger[3,7], BIG BEAR Consortium* and Gideon Nave[2]✉

Previous research points to the heritability of risk-taking behaviour. However, evidence on how genetic dispositions are translated into risky behaviour is scarce. Here, we report a genetically informed neuroimaging study of real-world risky behaviour across the domains of drinking, smoking, driving and sexual behaviour in a European sample from the UK Biobank (*N* = 12,675). We find negative associations between risky behaviour and grey-matter volume in distinct brain regions, including amygdala, ventral striatum, hypothalamus and dorsolateral prefrontal cortex (dlPFC). These effects are replicated in an independent sample recruited from the same population (*N* = 13,004). Polygenic risk scores for risky behaviour, derived from a genome-wide association study in an independent sample (*N* = 297,025), are inversely associated with grey-matter volume in dlPFC, putamen and hypothalamus. This relation mediates roughly 2.2% of the association between genes and behaviour. Our results highlight distinct heritable neuroanatomical features as manifestations of the genetic propensity for risk taking.

Taking risks—an essential element of many human experiences and achievements—requires balancing uncertain positive and negative outcomes. For instance, exploration, innovation and entrepreneurship can yield great benefits, but are also prone to failure[1]. Conversely, excessive risk taking in markets can have enormous societal costs, such as the generation of speculative price bubbles[2]. Similarly, common behaviours such as smoking, drinking, sexual promiscuity or speeding are considered rewarding by many but might expose individuals and those around them to deleterious health, social and financial consequences. In 2010, the combined economic burden in the United States of these risky behaviours was estimated to be about US$593.3 billion (refs. [3–6]). Although previous findings point to the partial heritability of risk tolerance and risky behaviours[7] and neuroanatomical measures exhibit high heritability[8,9], little is known about the brain features involved in translating genetic dispositions into risky behavioural phenotypes[8].

Recent research using structural brain-imaging data from small, non-representative samples (comprising up to a few hundred participants) has identified several neuroanatomical associations with risk tolerance[10–12]. However, this literature is limited by low statistical power[13,14], and the generalizability of their findings to other populations is questionable. Small sample sizes have also limited the ability to control systematically for many factors that could confound observed relations between brain features and risky behaviour, such as height[15] and genetic population structure[16,17]. Moreover, despite evidence that the effects of genetic factors are probably mediated by their influence on the brain and its development[7,18], neuroscientific and genetic approaches to understanding the biology of risky behaviour have largely proceeded in isolation—perhaps due to the lack of large study samples that include both genetic and brain-imaging measures.

Here, we use data obtained in a prospective epidemiological study of roughly 500,000 individuals aged 40 to 69 years (the UK Biobank (UKB)[19,20]) to carry out a preregistered investigation (https://osf.io/qkp4g/, see Supplementary Methods for deviations from the analysis plan) of the relationship between individual differences in brain anatomy and the propensity to engage in risky behaviour across four domains (N = 12,675, for sample characteristics see Fig. 1 and Extended Data Fig. 1). We replicate our findings in an independent sample recruited from the same population (N = 13,004, for sample characteristics see Extended Data Fig. 2). Further, we isolate specific differences in brain anatomy that are linked to the genetic disposition for risky behaviour—quantified via polygenic risk scores (PRS) derived from a genome-wide association study (GWAS) in an independent sample (N = 297,025)—and investigate how these neuroanatomical endophenotypes mediate the influence of genetics on the behavioural phenotype.

Results

Grey-matter volume (GMV) associations with risky behaviour. Akin to a previous investigation[7], we construct a measure of risky behaviour by extracting the first principal component from four self-reported measures of drinking, smoking, speeding on motorways and sexual promiscuity (N = 315,855, see Fig. 2a, Supplementary Methods and Supplementary Tables 1 and 2 for descriptive statistics). This measure of risky behaviour is genetically correlated with many other traits, including cannabis use (r_g = 0.72, s.e. = 0.02), general risk tolerance (r_g = 0.56, s.e. = 0.02), self-employment (r_g = 0.52, s.e. = 0.30), suicide attempt (r_g = 0.47, s.e. = 0.07), antisocial behaviour (r_g = 0.45, s.e. = 0.14), extraversion (r_g = 0.34, s.e. = 0.04) and age at first sexual experience (r_g = −0.54,

[1]Zurich Center for Neuroeconomics, Department of Economics, University of Zurich, Zurich, Switzerland. [2]Marketing Department, The Wharton School, University of Pennsylvania, Philadelphia, PA, USA. [3]Department of Economics, School of Business and Economics, Vrije Universiteit Amsterdam, Amsterdam, the Netherlands. [4]Department of Psychology, University of Pennsylvania, Philadelphia, PA, USA. [5]Department of Psychiatry, University of Pennsylvania Perelman School of Medicine, Philadelphia, PA, USA. [6]Veterans Integrated Service Network 4, Mental Illness Research, Education and Clinical Center, Crescenz Veterans Affairs Medical Center, Philadelphia, PA, USA. [7]La Follette School of Public Affairs, University of Wisconsin-Madison, Madison, WI, USA. *A full list of members and their affiliations appears in the Supplementary Information. ✉e-mail: gnave@wharton.upenn.edu

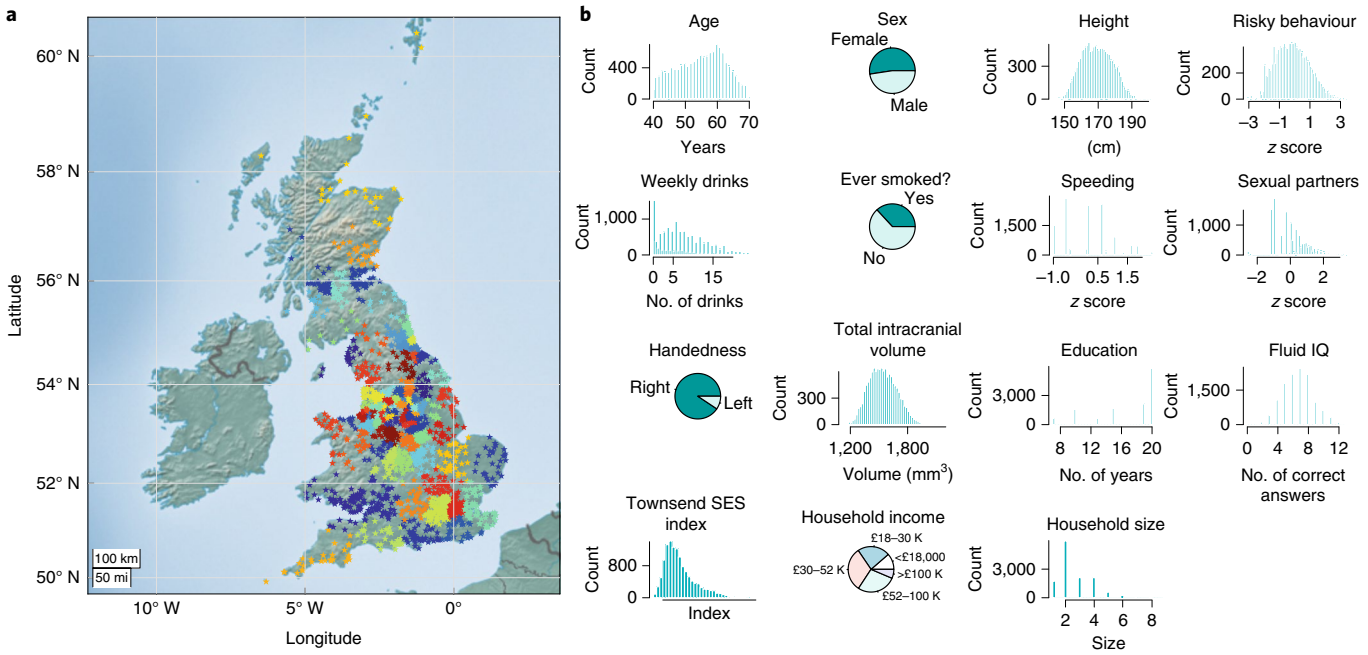

Fig. 1 | Main sample characteristics ($N = 12{,}675$). a, Geographical birth location clusters of the study's participants. Each star represents the birthplace of a participant (non-jittered). Colours denote 100 geographical clusters, calculated using a *k*-means clustering algorithm with $k = 100$ and 10,000 iterations after random seeding. **b**, Empirical distributions of variables in the main study sample.

s.e. = 0.02) (Supplementary Methods and Supplementary Table 3). Thus, our measure is partly rooted in genetic differences between people and relates to a broad range of relevant events and behaviours.

Our main analysis includes a sample of 12,675 European-ancestry participants from the UKB. We first regress our measure of risky behaviour on total (whole-brain) GMV while controlling for age, birth year, gender, handedness, height, total intracranial volume and the first 40 genetic principal components, which account for genetic population structure (Supplementary Methods). To exclude confounding effects of excessive alcohol consumption[21], we excluded from the analysis all current or former heavy drinkers (Methods)[22,23]. We find an inverse association between total GMV and risky behaviour (standardized $\beta = -0.122$; 95% confidence interval (CI) −0.156, −0.087; $t(12{,}561) = -6.92$; $P < 4.86 \times 10^{-12}$, two-sided).

To identify specific brain regions related to risky behaviour, we perform a whole-brain voxel-based morphometry (VBM)[24] analysis that regresses our measure of risky behaviour separately on GMV in each voxel across the brain, adjusting for the same control variables. We identify localized inverse associations between risky behaviour and GMV in distinct regions, only some of which were expected on the basis of previous small-scale studies (Fig. 2b, Extended Data Fig. 3 and Supplementary Table 4). In subcortical areas, we identify associations bilaterally in expected areas such as the amygdala and ventral striatum, as well as in less expected areas such as the posterior hippocampus, putamen, thalamus, hypothalamus and cerebellum. We also identify bilateral associations between risky behaviour and GMV in cortical regions that include the ventral medial prefrontal cortex (vmPFC), dorsolateral prefrontal cortex (dlPFC), ventro-anterior insula (aINS) and the precentral gyrus. In all of these regions, GMV is negatively associated with the propensity to engage in risky behaviours. We find no positive associations between GMV and risky behaviour anywhere in the brain.

To quantify effect sizes of the associations between risky behaviour and GMV in anatomically defined brain structures and to investigate the convergence of our findings across MRI processing pipelines[25], we conduct a follow-up analysis at the region of interest (ROI) level. This analysis primarily relies on the imaging-derived phenotypes (IDPs) provided by the UKB brain-imaging processing pipeline[8,26,27], which used parcellations from the Harvard–Oxford cortical and subcortical atlases and the Diedrichsen cerebellar atlas. We derived additional IDPs using unbiased masks on the basis of the results of the voxel-level analysis (Supplementary Methods). This analysis identifies negative associations between risky behaviour and GMV in 23 anatomical structures, with standardized βs between −0.079 and −0.036 (Fig. 2c, Extended Data Fig. 4 and Supplementary Table 5; for the associations between the IDPs and the individual measures that construct our phenotype of risky behaviour, see Supplementary Table 6), the largest of which is in the right ventro-aINS ($\beta = -0.079$; 95% CI −0.103, −0.055; $t(12{,}562) = -6.43$; $P_{uncorr} = 1.34 \times 10^{-10}$, two-sided).

We carry out several additional analyses to assess the differential contributions of various factors to the associations we observe. First, we re-estimate the ROI-level regressions with additional controls for various socioeconomic and cognitive outcomes that may be linked to both brain anatomy and risky behaviour, either as antecedents or downstream consequences. These controls include participants' years of education and fluid intelligence (13-item measure)[17], a zip-code level measure of the Townsend social deprivation index[28], household income and size, and birth location binned into 100 geographical clusters (Supplementary Methods and Fig. 1). The direction and magnitude of all ROI effects are comparable to the main analysis (range of standardized β between −0.079 and −0.035), with the largest effect again located in the right ventro-aINS ($\beta = -0.079$; 95% CI −0.104, −0.055; $t(11{,}647) = -6.29$; $P_{uncorr} = 3.3 \times 10^{-10}$, two-sided). Furthermore, 19 of the 23 ROI (all except the left cuneal cortex, left Crus I of the cerebellum, left planum polare and the brain stem) are statistically significant after correction for multiple comparisons in this analysis (Extended Data Fig. 5 and Supplementary Table 5).

Second, we re-estimate our ROI-level regressions with additional controls for current levels of drinking (binned into ten deciles) and

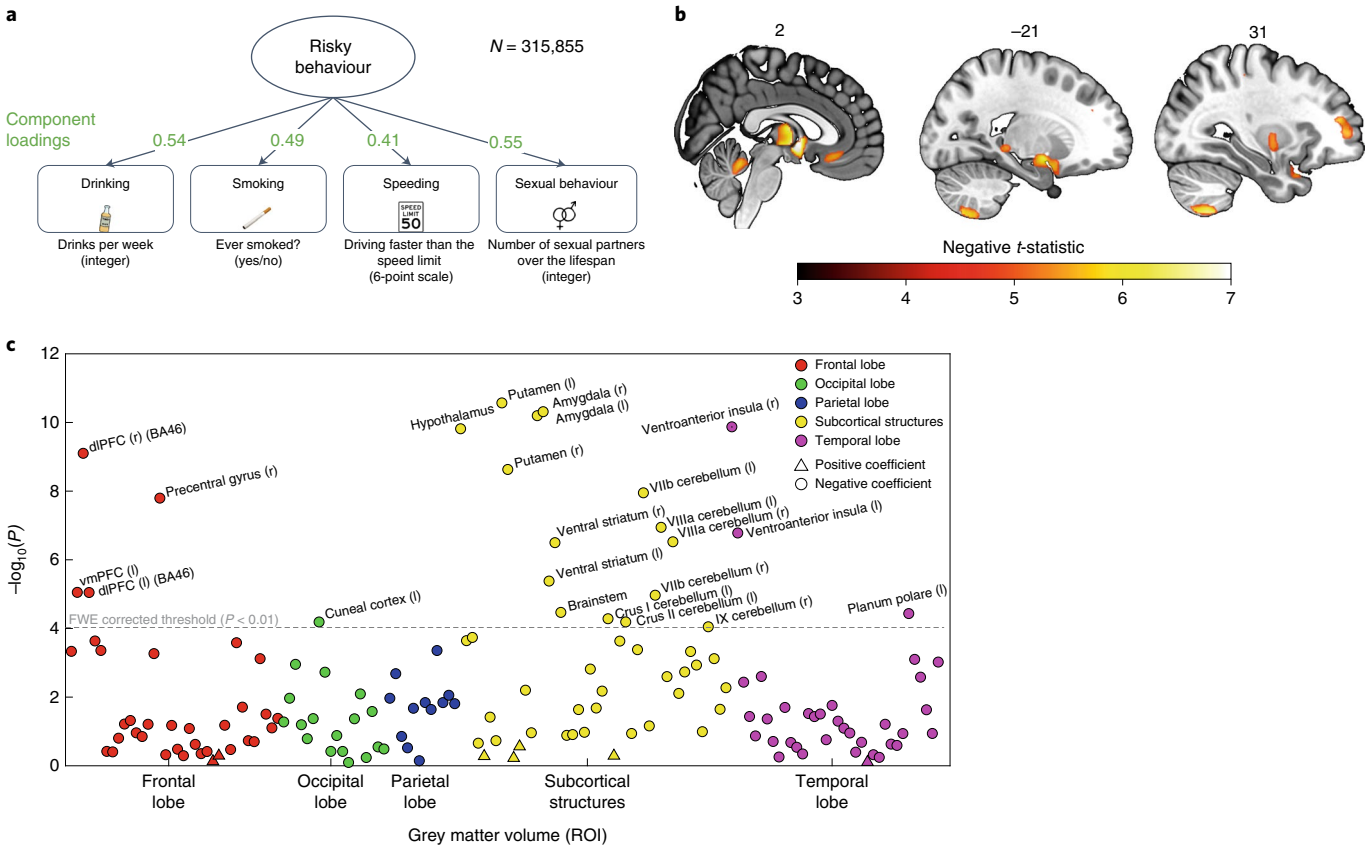

Fig. 2 | Association between risky behaviour and IDPs of GMV. a, Loadings for the first principal component are extracted from four self-reported measures of risky behaviour in the drinking, smoking, driving and sexual domains ($N = 315,855$) (see Fig. 1 for descriptive statistics). We use this first principal component as a measure of risky behaviour. **b**, Voxel-level GMV negatively associated with risky behaviour ($N = 12,675$). We observe associations in subcortical areas, including thalamus, posterior hippocampus, amygdala, putamen, ventral striatum and cerebellum. Associations with cortical areas include posterior middle temporal gyrus, precentral gyrus, dlPFC, anterior insula and vmPFC. **c**, Associations between risky behaviour and GMV in 148 ROI ($N = 12,675$). The grey dotted line shows the FWE-corrected threshold of $P = 0.01$ (see Methods for details).

smoking (binned into three categories). Although introducing these controls into the model regresses out variance of interest from the main outcome measure, which probably attenuates the effects, this analysis allows us to test whether any of the identified associations can reliably be attributed to risky behaviour that is not limited to the substance-use domain. In this analysis, we find that all of the effects originally identified remain negative in sign, yet are smaller in magnitude (range of standardized β values between −0.041 and −0.011; Supplementary Table 7). Nonetheless, the effects in nine subcortical ROI (including the amygdala, putamen, ventral striatum and cerebellum) remain statistically significant after correction for multiple comparisons (Extended Data Fig. 6), with the strongest association identified in the left amygdala ($\beta = -0.041$; 95% CI −0.059, −0.023; $t(12,551) = -4.4$; $P_{uncorr} = 1.1 \times 10^{-5}$, two-sided). Thus, these subcortical IDPs are reliably associated with risky behaviour in non-substance-use domains.

Replication in an independent sample. Several months after the completion of our original analyses (in February 2020, https://biobank.ndph.ox.ac.uk/showcase/exinfo.cgi?src=timelines), the UKB released brain images of 20,316 additional participants—providing us with an opportunity to replicate our findings in an independent dataset that contains the same variables, and participants recruited in the same way from the same population[29]. After applying the same exclusion criteria as in our original analysis, our replication sample consists of 13,004 participants, roughly the same size as our original sample (see Methods for details and Extended Fig. 1 for sample characteristics). We repeat both the voxel-level and ROI-level analyses in this dataset. In the voxel-level analysis, we apply a significance threshold that corresponds to a family-wise-error (FWE) rate of 5% in all voxels that showed significance in the original analysis ($P_{uncorr} = 2.956 \times 10^{-04}$, with $t_{uncorr}(12,892) = 3.62$, two-sided). We find that 92.6% of the original voxels (located in 20 of the 21 clusters originally identified, with the exception of a cluster in cerebellar lobules I–IV) successfully replicate (Fig. 3). Furthermore, the un-thresholded t-map[25] of the original dataset strongly correlates with the un-thresholded t-map of the replication dataset ($r = 0.767$; 95% CI 0.766, 0.768; $P < 10^{-10}$, two-sided). Likewise, our ROI-level analysis successfully replicates 21 of the original 23 ROI-level findings ($P_{uncorr} = 3.35 \times 10^{-03}$, with $t_{uncorr}(12,892) = 2.93$, two-sided; Supplementary Table 8). The two ROI that do not replicate are the cuneal cortex (left) and the cerebellar lobule II (left).

Overlap between GMV differences and functional MRI (fMRI) meta-analysis. To investigate whether the neuroanatomical associations of real-world risky behaviour correspond spatially with the localized activation patterns commonly identified in fMRI studies of risky decision-making, we conduct a conjunction analysis to compare our VBM results with data obtained from a publicly available meta-analysis of fMRI studies of risky behaviour[30] ($N = 4,717$ participants, $K = 101$ individual studies; Supplementary Table 9). The analysis reveals several brain regions whose anatomical

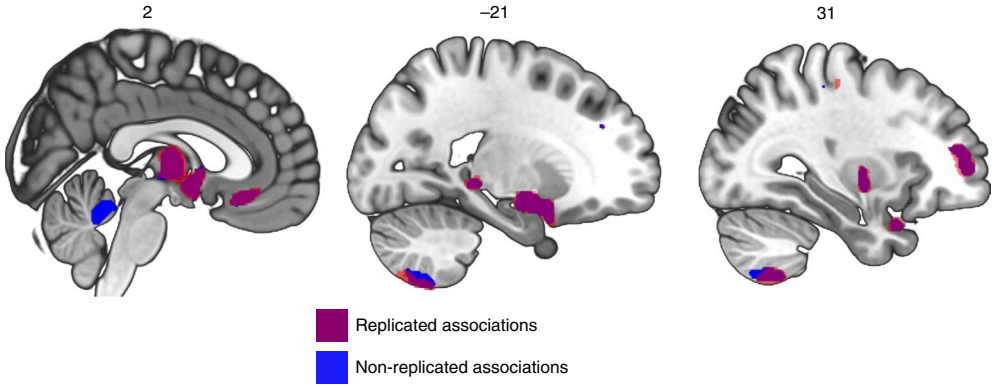

Fig. 3 | Voxel-level GMV associated with risky behaviour in the replication sample ($N = 13{,}004$). Here, 92.6% of the voxels identified in our original analysis (located in 20 of 21 original clusters identified, marked in purple) successfully replicate (corrected for multiple testing at the 5% level using a permutation test). Non-replicated voxels are located in the cerebellar lobules I–IV (marked in blue).

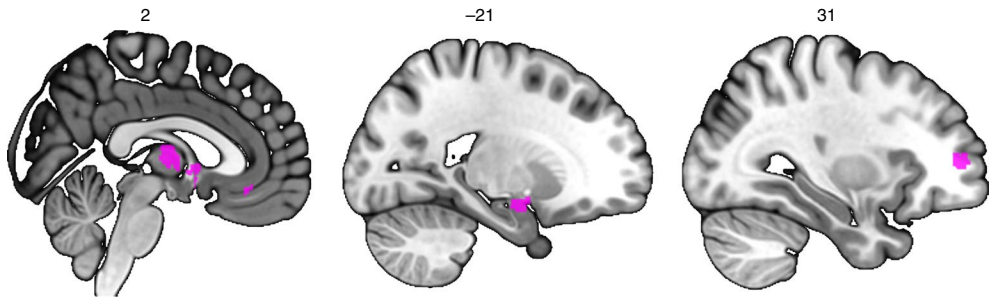

Fig. 4 | Conjunction between the GMV differences associated with risky behaviour identified in the current study and the results of a meta-analysis of 101 fMRI studies, on the basis of the keyword 'risky'. This analysis identifies overlapping voxels in the thalamus, amygdala, vmPFC and dlPFC (Methods).

associations with risky behaviour converge with functional engagement, including the thalamus, amygdala, vmPFC and dlPFC (Fig. 4 and Extended Data Fig. 7).

Association of PRS for risky behaviour with GMV. Finally, we explore whether participants' genetic disposition for risky behaviour, proxied via their PRS, are associated with the neuroanatomical correlates of the trait and test whether these neuroanatomical correlates mediate the relationship between genetic predisposition and behaviour. To this end, we first conducted a GWAS in an independent sample of UKB participants of European ancestry ($N = 297{,}025$), exclusive of 18,796 genotyped individuals with usable MRI images (main sample) and their relatives. From the GWAS, we constructed a PRS that aggregated the effects of 1,176,729 single-nucleotide polymorphisms (SNPs) on risky behaviour for all of the participants with MRI data in our independent target sample (Supplementary Methods). The PRS predict roughly 3% of the variance in risky behaviour in our target sample. Although we find no statistically significant evidence to suggest that the PRS are associated with whole-brain GMV (standardized $\beta = -0.015$; 95% CI −0.05 0.02; $t(12{,}561) = -0.82$; $P > 0.41$, two-sided), they are inversely associated with GMV in distinct regions, specifically the right dlPFC, right putamen and hypothalamus (Fig. 5a, regressions include all standard control variables, including total intracranial volume). Thus, GMV in these specific brain areas is negatively associated with the genetic disposition for risky behaviour.

On the basis of these results, we use the previously extracted GMV of these three ROI to examine whether it mediates the observed gene-behaviour associations. A structural equation model (SEM) including all standard controls reveals that roughly 2.2% of the association between the PRS and risky behaviour is mediated through individual differences in GMV in the three regions (indirect path c' standardized $\beta = 0.004$, 95%; CI 0.002, 0.005; $z = 4.83$; $P = 1.4 \times 10^{-06}$, two-sided) (Fig. 5b and Extended Data Fig. 8).

Discussion

We investigate, in a genetically informed neuroimaging study, (1) the association between GMV and real-world risky behaviour in a large population sample of European ancestry (main sample of 12,675 individuals and replication sample of 13,004 individuals), and (2) how the genetic disposition for risky behaviour is linked to GMV differences in a network of distinct brain areas. Several of the areas whose GMVs are linked to risky behaviour in this study have also often been functionally engaged during risky decision-making in small-scale fMRI studies that used stylized tasks. For instance, such correlations have been observed in the aINS, thalamus, dlPFC, vmPFC and ventral striatum[31,32]. These findings have led to proposals that upward and downward risks are encoded by distinct circuits, with upward risk mainly represented by areas encoding rewards (ventral striatum and vmPFC) and downward risk encoded by areas related to avoidance and negative arousal (aINS). Here, we substantiate previous functional studies with large-scale evidence that the structural properties of the same areas relate to risky behaviour in an ecologically valid setting[33] when long-term health consequences are at stake.

Our results extend previous findings by showing that the neural foundation of risky behaviour is complex. Our analyses identify additional negative associations between risky behaviour and GMV in several areas, including the cerebellum, posterior hippocampus, hypothalamus and putamen. While it is not yet clear how

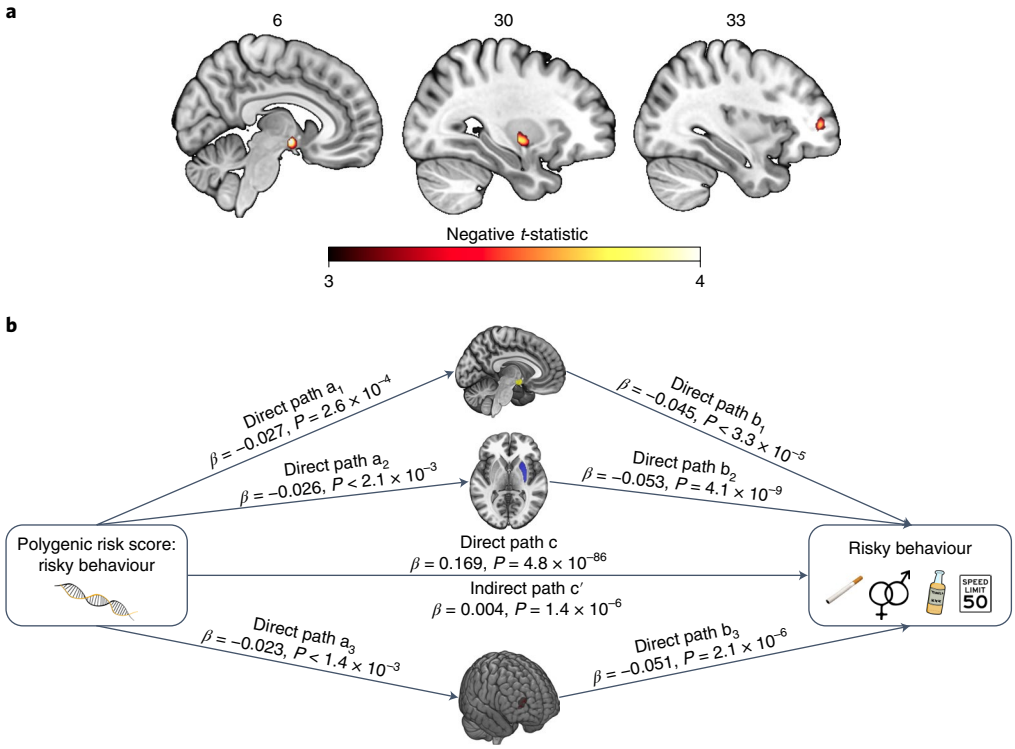

Fig. 5 | Association of PRS for risky behaviour and GMV. a, We constructed PRS of risky behaviour from a GWAS in an independent sample (N = 297,025) and investigated their associations with GMV in brain voxels that we identified as linked to risky behaviour. The PRS negatively correlate with GMV in the right dlPFC, putamen and hypothalamus. **b**, GMV differences in hypothalamus (path 1, designated as a_1 and b_1), right putamen (path 2, designated as a_2 and b_2) and right dlPFC (path 3, designated as a_3 and b_3) mediate roughly 2.2% of the association between the PRS and risky behaviour. Arrows depict the direction of the SEM and do not indicate causality (N = 12,675).

structural differences are manifested in properties of brain function[34], our results suggest that risk taking draws on manifold neural processes, not just the representation and integration of upward and downward risks in the brain. Specifically, considering previous meta-analyses, the areas identified in this study are involved broadly in memory (posterior hippocampus), emotion processing (amygdala, ventro-aINS)[35], neuroendocrine processes (hypothalamus)[36,37], reward processing (vmPFC, ventral striatum and putamen)[38] and executive functions (dlPFC)[39]. Thus, it appears that risky behaviour taps into multiple elements of human cognition, ranging from inhibitory control[40] to emotion regulation[41] and the integration of outcomes and risks[42]. This mirrors previous findings showing that risky behaviour is also a genetically complex trait[7].

Additionally, our results underscore the long-suspected role of the hypothalamic–pituitary–adrenal axis in regulating risk-related behaviours, in line with hormonal studies that link risky behaviour and sensation seeking to stress responsivity[36,37,43–45]. Furthermore, our finding that risky behaviour is linked to the structure of several cerebellar areas confirms the under-appreciated importance of the cerebellum for human cognition and decision-making, and highlights the need for further research on the specific behavioural contributions of this brain area[46].

Of note, it remains an open question the extent to which the differences in GMV that we identify can be ascribed to specific heritable micro-anatomical traits, such as neuronal size, dendritic or axonal arborization, or relative count of different cell types[47]. Moreover, it is not yet clear how these individual differences, in turn, influence behaviour. Nonetheless, our results provide evidence that neuroanatomical structure constitutes the micro-foundation for neuro-computational mechanisms underlying individual differences in risky behaviours[34].

Several of the observed neuroanatomical correlates of risky behaviour are also associated with the genetic disposition for the phenotype. Specifically, we find that GMV in the hypothalamus, the putamen and the dlPFC share variance with both risky behaviour and its PRS. This finding extends previous studies showing correlational[36,42,43] and causal evidence[37,48] of the involvement of these areas in risky behaviour by indicating that a genetic component partly underlies the associations. Although our analyses cannot identify the direction of the causal relationships (see Supplementary Discussion for an additional discussion of limitations), they show that risky behaviour and its genetic associations share variance with distinct GMV features and provide an overarching framework for how the genetic dispositions for risky behaviour may be expressed in the corresponding behavioural phenotype.

Our results are also in line with the bioinformatic annotation of the largest GWAS on risk tolerance until now, conducted in over 1 million individuals[7], which implicated specific areas in the prefrontal cortex (BA9, BA24), striatum, cerebellum and the amygdala. However, bioinformatics tools used for GWAS annotation cannot be considered conclusive, as they rely on gene expression patterns in relatively small samples of (post mortem) human brains or non-human samples[49]. Moreover, they cannot speak to whether changes in a particular tissue or cell type have negative or positive effects on the phenotype or how strong the effects are. Here, we show an alternative approach to annotating GWAS findings using a different type of data (large-scale population samples that include in vivo brain scans and genetic data), relying on different assumptions from those used by bioinformatics tools. Our results add new insight by showing that lower GMV in specific brain areas is related to more risky behaviour and by implicating brain regions (that is, putamen, hypothalamus and dlPFC) in addition to those previously

annotated. The effect sizes we observe here (standardized $\beta < 0.08$) are an order of magnitude larger than those found in GWAS on risky behaviour, but they nonetheless require very large samples for detection.

Finally, while many features of the brain are heritable, the environment indisputably plays an important role in brain development. We therefore see our results not as independent from, or of greater importance than, the effects of environmental and developmental factors. Rather, our study constitutes one step towards understanding how the complex development of human risky behaviour may be constrained by genetic factors.

Methods

Sample characteristics and selection criteria. *Main sample.* We use publicly available data from the UKB, which recruited 502,617 people aged 40 to 69 years from the general population across the United Kingdom[19,20]. All UKB participants provided written informed consent and the study was granted ethical approval by the North West Multi-Centre Ethics committee. Our initial sample consists of 18,796 individuals with brain scans and genotype data, all of the imaged UKB participants as of October 2018. We excluded participants with putative sex chromosome aneuploidy ($N=6$) or a mismatch between genetic and reported sex ($N=10$), participants of non-European ancestry ($N=893$) and participants who did not pass the UKB quality-control thresholds ($N=14$), described in Bycroft et al.[27]. To minimize the potential influence of neurotoxic effects due to excessive alcohol intake[21,22], we also excluded current heavy drinkers (531 females consuming more than 18 drinks per week and 793 males consuming more than 24 drinks per week)[22,23]. To exclude potential former drinkers, we also removed 426 participants who indicated that they did not drink alcohol.

All structural T1 MRI images used in the study underwent automated quality control by the UKB brain-imaging processing pipeline[26]. We performed two additional quality checks using the Computational Anatomy Toolbox (CAT, www.neuro.uni-jena.de/cat/) for SPM 12 (www.fil.ion.ucl.ac.uk/spm/software/spm12/). First, we relied on the CAT12 automated image and preprocessing quality assessment, which included quality parameters for resolution, noise and bias of images, 57 of which were automatically excluded and not preprocessed due to low image quality. Second, after preprocessing, we used an automated quality check of sample homogeneity to identify outliers that exhibited substantially different GMV patterns from the rest of the sample (see the CAT12 manual for details at http://www.neuro.uni-jena.de/cat12/CAT12-Manual.pdf, p. 17ff). In total, we excluded 690 individuals with scans of high image inhomogeneity (two standard deviations below the mean). Finally, we excluded 2,701 participants with incomplete behavioural data of interest or control variables. Our final dataset consists of $N=12,675$ individuals.

Replication sample. The initial replication sample consisted of 20,316 individuals with usable brain scans and genotype data, all of the imaged UKB participants as of February 2020 who were not included in our main sample. Following the original analysis, we excluded participants with putative sex chromosome aneuploidy ($N=7$), a mismatch between genetic and reported sex ($N=11$), non-European ancestry ($N=1,143$), heavy drinking or abstinence from alcohol ($N=1,376$) and those that did not pass the UKB quality-control thresholds ($N=31$)[27]. All T1 MRI images used in the study underwent the same quality-control procedure as in our original sample, resulting in the removal of additional 391 individuals. Finally, we excluded participants with incomplete data ($N=4,353$). Our final replication sample consists of $N=13,004$. The empirical distributions of the variables characterizing our replication analysis are depicted in Extended Data Fig. 2.

Measures. *Risky behaviour.* We closely follow Karlsson Linnér et al.[7] to derive a measure of risky behaviour across domains on the basis of participants' self-reports of: (1) number of alcoholic drinks per week, (2) ever having smoked, (3) number of sexual partners and (4) frequency of driving faster than the motorway speed limit (Supplementary Methods). We perform principal component analysis on $N=315,855$ UKB participants and extract the first principal component of the four measures as the main outcome of interest (referred to as 'risky behaviour'). The first principal component explains roughly 37% of the variance in the four measures, and it is the only principal component that loads positively on all of them. Summary statistics and factor loadings of the principal component analysis are available in Supplementary Tables 1 and 2. The code for generating the variable of 'risky behaviour' is accessible at https://osf.io/qkp4g/.

Control variables. The full list of control variables and the methods used to generate them are available in Supplementary Methods.

T1 MRI image processing. We use T1-weighted structural brain MRI images in NIFTI format provided by the UKB. Images were acquired using 3-T Siemens Skyra scanners, with a 32-channel head coil (Siemens), with the following scanning parameters: repetition time, 2,000 ms; echo time, 2.1 ms; flip angle, 8°; matrix size, 256×256 mm^2; voxel size, $1 \times 1 \times 1$ mm^3 and number of slices, 208. A detailed description of the methods used to preprocess the images and derive voxel-level and ROI-level IDPs is available in Supplementary Methods.

PRS for risky behaviour. To construct PRS, we first re-estimated the GWAS of our main measure described in ref. [7] after excluding 18,796 genotyped individuals with usable T1 MRI images and their relatives up to the third degree (final GWAS sample, $N=297,025$ individuals of European ancestry). The GWAS was performed using linear mixed models, implemented via BOLT-LMM v.2.3.2 (ref. [50]). Next, we performed quality control of the GWAS results using a standardized quality control protocol, described in detail in ref. [7]. This protocol removes rare and low-quality SNPs on the basis of a minor allele frequency (MAF) of <0.001, imputation quality (INFO) of <0.7 and SNPs that could not be aligned with the Haplotype Reference Consortium reference panel, among other filters. After quality control, a total of 11,514,220 SNPs remained in the GWAS summary statistics. Thereafter, we calculated PRS for each participant by weighting their genotype across SNPs by the corresponding regression coefficients estimated in the GWAS (see Supplementary Methods for further information).

Analysis. *VBM.* We identify associations between risky behaviour and localized GMV across the brain using whole-brain VBM, a method that normalizes the anatomical brain images of all participants in one stereotactic space[24]. We regress risky behaviour separately on each voxel of the smoothed GMV images (Supplementary Methods) and the control variables. We correct for multiple comparisons by adjusting the FWE rate to $\alpha=0.01$ using permutation tests ($P_{\text{uncorr}}=1.248\times10^{-06}$, with $|t_{\text{uncorr}}|=4.85$, two-sided). See Extended Data Fig. 3 and Supplementary Table 4 for the summary statistics of each cluster and the coordinates of the peak voxel within that cluster.

ROI-level analysis. We compute the associations between risky behaviour and 139 IDPs of GMV extracted by the UKB brain-imaging processing pipeline[26] using parcellations from the Harvard–Oxford cortical and subcortical atlases and Diedrichsen cerebellar atlas, in addition to nine IDPs derived using unbiased masks on the basis of the results of our voxel-level analysis (Supplementary Methods). We regress risky behaviour separately on each IDP and the control variables and correct for multiple comparisons by adjusting the FWE rate of $\alpha=0.01$ using permutation tests ($P_{\text{uncorr}}=9.37\times10^{-05}$, with $|t_{\text{uncorr}}|=3.91$, two-sided).

Replication of the voxel-level and ROI-level analyses. We repeat the VBM analyses in the replication sample for all voxels that showed significance in the original sample, correcting for multiple comparisons by adjusting the FWE rate to $\alpha=0.05$ (two-tailed) using permutation tests ($P_{\text{uncorr}}=2.956\times10^{-04}$, with $t_{\text{uncorr}}=3.62$). We also repeat the ROI-level analysis in all ROI that showed significance in the original sample, and correct for multiple comparisons by adjusting the FWE rate to $\alpha=0.05$ (two-tailed) using permutation tests ($P_{\text{uncorr}}=3.35\times10^{-03}$, with $t_{\text{uncorr}}=2.93$). We define replication success as observing a statistically significant effect at the 5% level (corrected for multiple hypothesis testing) in the same direction as the original finding[51].

Comparison of VBM Results with a meta-analysis of fMRI studies. We compare our VBM results with a publicly available meta-analysis of fMRI studies provided by Neurosynth[30], an online platform for large-scale, automated synthesis of fMRI data (https://neurosynth.org/). The meta-analysis was based on the keyword 'risky'. It consisted of $K=101$ individual studies with a total of $N=4,717$ participants (see Supplementary Table 9 for details), and was conducted using a uniformity test (assuming that random activations are evenly distributed across all voxels). The meta-analytic statistical image was corrected for multiple comparisons by applying a false discovery rate of 0.01 (implemented by Neurosynth). The summary of studies included in the meta-analysis is available in Supplementary Table 9. The 3D activation map that resulted from the meta-analysis is available at https://neurosynth.org/analyses/terms/risky/. To compare our VBM results (that is, brain structure) with the meta-analysis of data on brain function, we perform a whole-brain voxel-level conjunction analysis of the two (Extended Data Fig. 7) that exhibits the spatial overlap of all voxels that are significant in both analyses (Fig. 4). Thus, both the structure and function of the brain regions identified by this conjunction are significantly associated with risky behaviour.

VBM analysis of risky behaviour PRS. We repeat the VBM analysis in all voxels identified to be associated with risky behaviour, using the PRS as the dependent variable. This approach allows the identification of brain regions that were likely to mediate the effect of genetic disposition on risky behaviour. The PRS were constructed using GWAS results from an independent sample, to ensure that the effect size estimates in this analysis are not inflated due to overfitting. We account for multiple comparisons using a permutation test with an FWE rate of $P_{\text{FWE}}<0.05$. This part of the analysis was not preregistered.

Mediation analysis. We conduct mediation analyses (implemented in STATA 14) to test whether GMV differences in the brain regions whose GMVs are associated

with the PRS of risky behaviour (right dlPFC, right putamen and hypothalamus) mediate the association between the PRS and risky behaviour. We first extract GMV from these three ROI using the same unbiased masks as in the ROI-level analysis (Supplementary Methods). Then, we estimate a SEM to quantify the effect of the PRS on risky behaviour mediated via GMV differences in these ROI. All SEM equations include the aforementioned standard control variables (listed in Supplementary Methods). We carry out an additional robustness check by estimating an SEM that assumes one single path (that is, the sum of all ROI), which yields the same pattern of results (Extended Data Fig. 8).

FWE correction using permutation tests. To account for multiple hypothesis testing, we determine the appropriate FWE-corrected *P* value threshold with a permutation test procedure in each of our analyses[52]. To this end, we generated 1,000 datasets with randomly permuted phenotypes (that is, breaking the link between the outcome and explanatory variables), estimated regression models for all IDPs per analysis and recorded the lowest *P* value of each run to generate an empirical distribution of the test statistic under the null hypothesis. To obtain the FWE rate of any given alpha, we use the $n\text{th} = \alpha \times 1{,}000$ lowest *P* value from the 1,000 permutation runs as the FWE-corrected *P* value threshold.

Preregistration of analysis plan and unplanned deviations. We preregistered our analysis plan on the Open Science Framework (https://osf.io/qkp4g/, registered December 2018). Our preregistered plan specified the construction of the dependent variable, the control variables, the inclusion criteria and quality controls, the VBM analyses and the main ROI-level analyses. We summarize all deviations from the analysis plan in Supplementary Methods.

Reporting Summary. Further information on research design is available in the Nature Research Reporting Summary linked to this article.

Data availability

Data and materials are available via UKB at http://www.ukbiobank.ac.uk/.

Code availability

The analysis code used in this study is publicly available at https://osf.io/qkp4g/.

Received: 10 December 2019; Accepted: 26 November 2020;
Published online: 28 January 2021

References

1. Knight, F. H. *Risk, Uncertainty, and Profit* (Houghton Mifflin, 1921).
2. Eckel, C. C. & Füllbrunn, S. C. Thar SHE blows? gender, competition, and bubbles in experimental asset markets. *Am. Economic Rev.* **105**, 906–920 (2015).
3. *Incidence, Prevalence, and Cost of Sexually Transmitted Infections in the United States* (Centers for Disease Control and Prevention, 2013); https://www.cdc.gov/std/stats/sti-estimates-fact-sheet-feb-2013.pdf
4. Sacks, J. J., Gonzales, K. R., Bouchery, E. E., Tomedi, L. E. & Brewer, R. D. 2010 national and state costs of excessive alcohol consumption. *Am. J. Prev. Med.* **49**, e73–e79 (2015).
5. Blincoe, L., Miller, T. R., Zaloshnja, E. & Lawrence, B. A. *The Economic and Societal Impact of Motor Vehicle Crashes, 2010 (revised)* (Transportation Research Board, 2015); https://trid.trb.org/view/1311862
6. *The Health Consequences of Smoking: 50 Years of Progress. A Report of the Surgeon General. Atlanta, GA* (US Department of Health and Human Services, Centers for Disease Control and Prevention, National Center for Chronic Disease Prevention and Health Promotion, Office on Smoking and Health, 2014).
7. Karlsson Linnér, R. et al. Genome-wide association analyses of risk tolerance and risky behaviors in over 1 million individuals identify hundreds of loci and shared genetic influences. *Nat. Genet.* **51**, 245–257 (2019).
8. Elliott, L. T. et al. Genome-wide association studies of brain imaging phenotypes in UK Biobank. *Nature* **562**, 210–216 (2018).
9. Thompson, P. M. et al. Genetic influences on brain structure. *Nat. Neurosci.* **4**, 1253–1258 (2001).
10. Grubb, M. A., Tymula, A., Gilaie-Dotan, S., Glimcher, P. W. & Levy, I. Neuroanatomy accounts for age-related changes in risk preferences. *Nat. Commun.* **7**, 13822 (2016).
11. Jung, W. H., Lee, S., Lerman, C. & Kable, J. W. Amygdala functional and structural connectivity predicts individual risk tolerance. *Neuron* **98**, 394–404. e4 (2018).
12. Nasiriavanaki, Z. et al. Prediction of individual differences in risky behavior in young adults via variations in local brain structure. *Front. Neurosci.* **9**, 359 (2015).
13. Button, K. S. et al. Power failure: why small sample size undermines the reliability of neuroscience. *Nat. Rev. Neurosci.* **14**, 365–376 (2013).
14. Marek, S. et al. Towards reproducible brain-wide association studies. Preprint at *bioRxiv* https://doi.org/10.1101/2020.08.21.257758 (2020).
15. Dohmen, T. et al. Individual risk attitudes: measurement, determinants, and behavioral consequences. *J. Eur. Economic Assoc.* **9**, 522–550 (2011).
16. Cardon, L. R. & Palmer, L. J. Population stratification and spurious allelic association. *Lancet* **361**, 598–604 (2003).
17. Nave, G., Jung, W. H., Karlsson Linnér, R., Kable, J. W. & Koellinger, P. D. Are bigger brains smarter? Evidence from a large-scale preregistered study. *Psychol. Sci.* **30**, 43–54 (2019).
18. Romer, D. Adolescent risk taking, impulsivity, and brain development: implications for prevention. *Dev. Psychobiol.* **52**, 263–276 (2010).
19. Miller, K. L. et al. Multimodal population brain imaging in the UK Biobank prospective epidemiological study. *Nat. Neurosci.* **19**, 1523–1536 (2016).
20. Sudlow, C. et al. UK Biobank: an open access resource for identifying the causes of a wide range of complex diseases of middle and old age. *PLoS Med.* **12**, e1001779 (2015).
21. Harper, C. The neurotoxicity of alcohol. *Hum. Exp. Toxicol.* **26**, 251–257 (2007).
22. Daviet, R. et al. Multimodal brain imaging study of 36,678 participants reveals adverse effects of moderate drinking. Preprint at *bioRxiv* https://doi.org/10.1101/2020.03.27.011791 (2020).
23. Kranzler, H. R. et al. Topiramate treatment for heavy drinkers: moderation by a GRIK1 polymorphism. *Am. J. Psychiatry* **171**, 445–452 (2014).
24. Ashburner, J. & Friston, K. J. Voxel-based morphometry—the methods. *Neuroimage* **11**, 805–821 (2000).
25. Botvinik-Nezer, R. et al. Variability in the analysis of a single neuroimaging dataset by many teams. *Nature* **582**, 84–88 (2020).
26. Alfaro-Almagro, F. et al. Image processing and quality control for the first 10,000 brain imaging datasets from UK Biobank. *Neuroimage* **166**, 400–424 (2018).
27. Bycroft, C. et al. The UK Biobank resource with deep phenotyping and genomic data. *Nature* **562**, 203–209 (2018).
28. Hill, W. D. et al. Molecular genetic contributions to social deprivation and household income in UK Biobank. *Curr. Biol.* **26**, 3083–3089 (2016).
29. Masouleh, S. K., Eickhoff, S. B., Hoffstaedter, F., Genon, S. & The Alzheimer's Disease NeuroImaging Initiative. Empirical examination of the replicability of associations between brain structure and psychological variables. *eLife* **8**, e43464 (2019).
30. Yarkoni, T., Poldrack, R. A., Nichols, T. E., Van Essen, D. C. & Wager, T. D. Large-scale automated synthesis of human functional neuroimaging data. *Nat. Methods* **8**, 665–670 (2011).
31. Mohr, P. N. C., Biele, G. & Heekeren, H. R. Neural processing of risk. *J. Neurosci.* **30**, 6613–6619 (2010).
32. Wu, C. C., Sacchet, M. D. & Knutson, B. Toward an affective neuroscience account of financial risk taking. *Front. Neurosci.* **6**, 159 (2012).
33. Schonberg, T., Fox, C. R. & Poldrack, R. A. Mind the gap: bridging economic and naturalistic risk-taking with cognitive neuroscience. *Trends Cogn. Sci.* **15**, 11–19 (2011).
34. Kable, J. W. & Levy, I. Neural markers of individual differences in decision-making. *Curr. Opin. Behav. Sci.* **5**, 100–107 (2015).
35. Chang, L. J., Yarkoni, T., Khaw, M. W. & Sanfey, A. G. Decoding the role of the insula in human cognition: functional parcellation and large-scale reverse inference. *Cereb. Cortex* **23**, 739–749 (2013).
36. Evans, B. E., Greaves-Lord, K., Euser, A. S., Franken, I. H. A. & Huizink, A. C. The relation between hypothalamic-pituitary-adrenal (HPA) axis activity and age of onset of alcohol use. *Addiction* **107**, 312–322 (2012).
37. Kreek, M. J., Nielsen, D. A., Butelman, E. R. & LaForge, K. S. Genetic influences on impulsivity, risk taking, stress responsivity and vulnerability to drug abuse and addiction. *Nat. Neurosci.* **8**, 1450–1457 (2005).
38. O'Doherty, J. et al. Dissociable roles of ventral and dorsal striatum in instrumental conditioning. *Science* **304**, 452–454 (2004).
39. Dosenbach, N. U. F., Fair, D. A., Cohen, A. L., Schlaggar, B. L. & Petersen, S. E. A dual-networks architecture of top-down control. *Trends Cogn. Sci.* **12**, 99–105 (2008).
40. Ivanov, I., Schulz, K. P., London, E. D. & Newcorn, J. H. Inhibitory control deficits in childhood and risk for substance use disorders: a review. *Am. J. Drug Alcohol Abus.* **34**, 239–258 (2008).
41. Heilman, R. M., Crişan, L. G., Houser, D., Miclea, M. & Miu, A. C. Emotion regulation and decision making under risk and uncertainty. *Emotion* **10**, 257–265 (2010).
42. Tobler, P. N., Christopoulos, G. I., O'Doherty, J. P., Dolan, R. J. & Schultz, W. Risk-dependent reward value signal in human prefrontal cortex. *Proc. Natl Acad. Sci. USA* **106**, 7185–7190 (2009).
43. Huizink, A. C., Ferdinand, R. F., Ormel, J. & Verhulst, F. C. Hypothalamic-pituitary-adrenal axis activity and early onset of cannabis use. *Addiction* **101**, 1581–1588 (2006).
44. Margittai, Z. et al. Combined effects of glucocorticoid and noradrenergic activity on loss aversion. *Neuropsychopharmacology* **43**, 334–341 (2018).
45. Grotzinger, A. D. et al. Hair and salivary testosterone, hair cortisol, and externalizing behaviors in adolescents. *Psychol. Sci.* **29**, 688–699 (2018).

46. Buckner, R. L. The cerebellum and cognitive function: 25 years of insight from anatomy and neuroimaging. *Neuron* **80**, 807–815 (2013).
47. Mechelli, A., Price, C. J., Friston, K. J. & Ashburner, J. Voxel-based morphometry of the human brain: methods and applications. *Curr. Med. Imaging Rev.* **1**, 105–113 (2005).
48. Knoch, D. et al. Disruption of right prefrontal cortex by low-frequency repetitive transcranial magnetic stimulation induces risk-taking behavior. *J. Neurosci.* **26**, 6469–6472 (2006).
49. *BrainSpan Atlas of the Developing Human Brain* (Allen Institute for Brain Science, 2015); http://www.brainspan.org/
50. Loh, P. et al. Efficient Bayesian mixed-model analysis increases association power in large cohorts. *Nat. Genet.* **47**, 284–290 (2015).
51. Camerer, C. F. et al. Evaluating the replicability of social science experiments in *Nature* and *Science* between 2010 and 2015. *Nat. Hum. Behav.* **2**, 637–644 (2018).
52. Dickie, D. A. et al. Permutation and parametric tests for effect sizes in voxel-based morphometry of gray matter volume in brain structural MRI. *Magn. Reson. Imaging* **33**, 1299–1305 (2015).

Acknowledgements

This research was carried out under the auspices of the Brain Imaging and Genetics in Behavioural Research (https://big-bear-research.org/) consortium. We thank N.C. Furtner for helpful comments and D. Manfredi for research assistance. The research was conducted using UKB resources under application no. 40830. The study was supported by funding from an National Science Foundation Early Career Development Program grant (no. 1942917) and The Wharton School Dean's Research fund to G.N., a European Research Council Consolidator grant to P.D.K. (no. 647648 EdGe), and a European Research Council Consolidator grant (no. 725355 BRAINCODES) and a Swiss National Science Foundation grant (no. 100019L_173248) to C.C.R . R.R.W. was financially supported by NIAAA K23 grant (no. K23 AA023894) and H.R.K. was supported by National Institute of Drug Abuse grant no. P30 DA046345. G.N. thanks C. and R. de la Cruz for ongoing support. The work was carried out on the Dutch national e-infrastructure with the support of the SURF Cooperative. The funders had no role in study design, data collection and analysis, decision to publish or preparation of the manuscript. Data can be accessed via the UK Biobank, and data analysis scripts are available on the Open Science Framework (https://osf.io/qkp4g/).

Author contributions

G.A., R.D., J.W.K., P.D.K. and G.N. designed the research plan. G.N., P.D.K. and C.C.R. oversaw the study. G.A., R.D. and R.K.L. analysed the data with critical input from P.D.K., G.N. and C.C.R. G.A., G.N. and P.D.K. wrote the paper and Supplementary Materials. T.A.H., H.R.K. and R.R.W. contributed to and critically reviewed the manuscript.

Competing interests

H.R.K. is a member of an advisory board for Dicerna Pharmaceuticals; a member of the American Society of Clinical Psychopharmacology's Alcohol Clinical Trials Initiative, which was sponsored in the past three years by AbbVie, Alkermes, Amygdala Neurosciences, Arbor Pharmaceuticals, Ethypharm, Indivior, Lilly, Lundbeck, Otsuka and Pfizer; and is named as an inventor on PCT patent application no. 15/878,640, entitled 'Genotype-guided dosing of opioid agonists' and filed 24 January 2018. All other authors declare no competing interests.

Additional information

Extended data is available for this paper at https://doi.org/10.1038/s41562-020-01027-y.

Supplementary information is available for this paper at https://doi.org/10.1038/s41562-020-01027-y.

Correspondence and requests for materials should be addressed to G.N.

Peer review information *Nature Human Behaviour* thanks Michelle Luciano, Agnieszka Tymula and the other, anonymous, reviewers for their contribution to the peer review of this work. Peer reviewer reports are available. Primary Handling Editor: Marike Schiffer.

Reprints and permissions information is available at www.nature.com/reprints.

Publisher's note Springer Nature remains neutral with regard to jurisdictional claims in published maps and institutional affiliations.

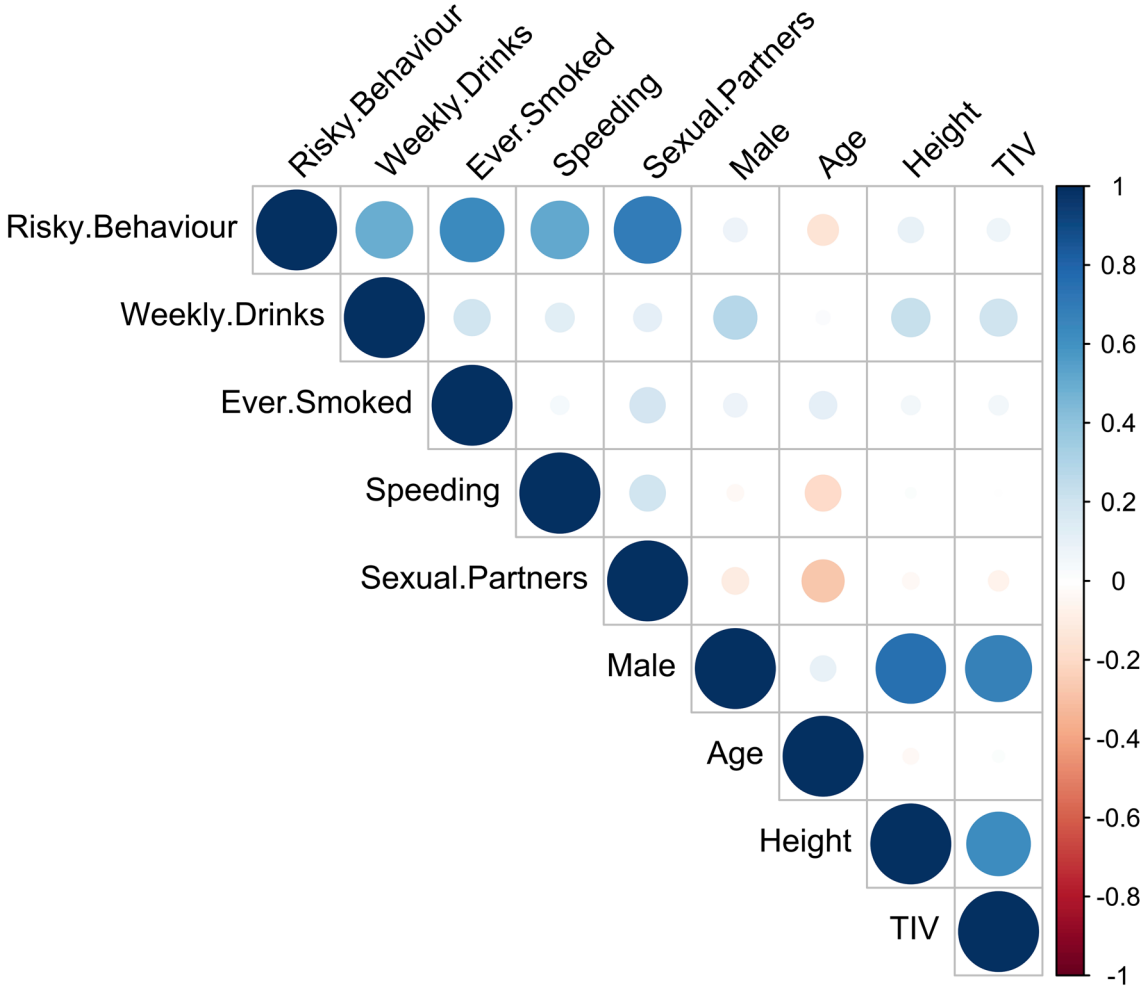

Extended Data Fig. 1 | Bivariate correlations between variables used in the main study sample (N = 12,675).

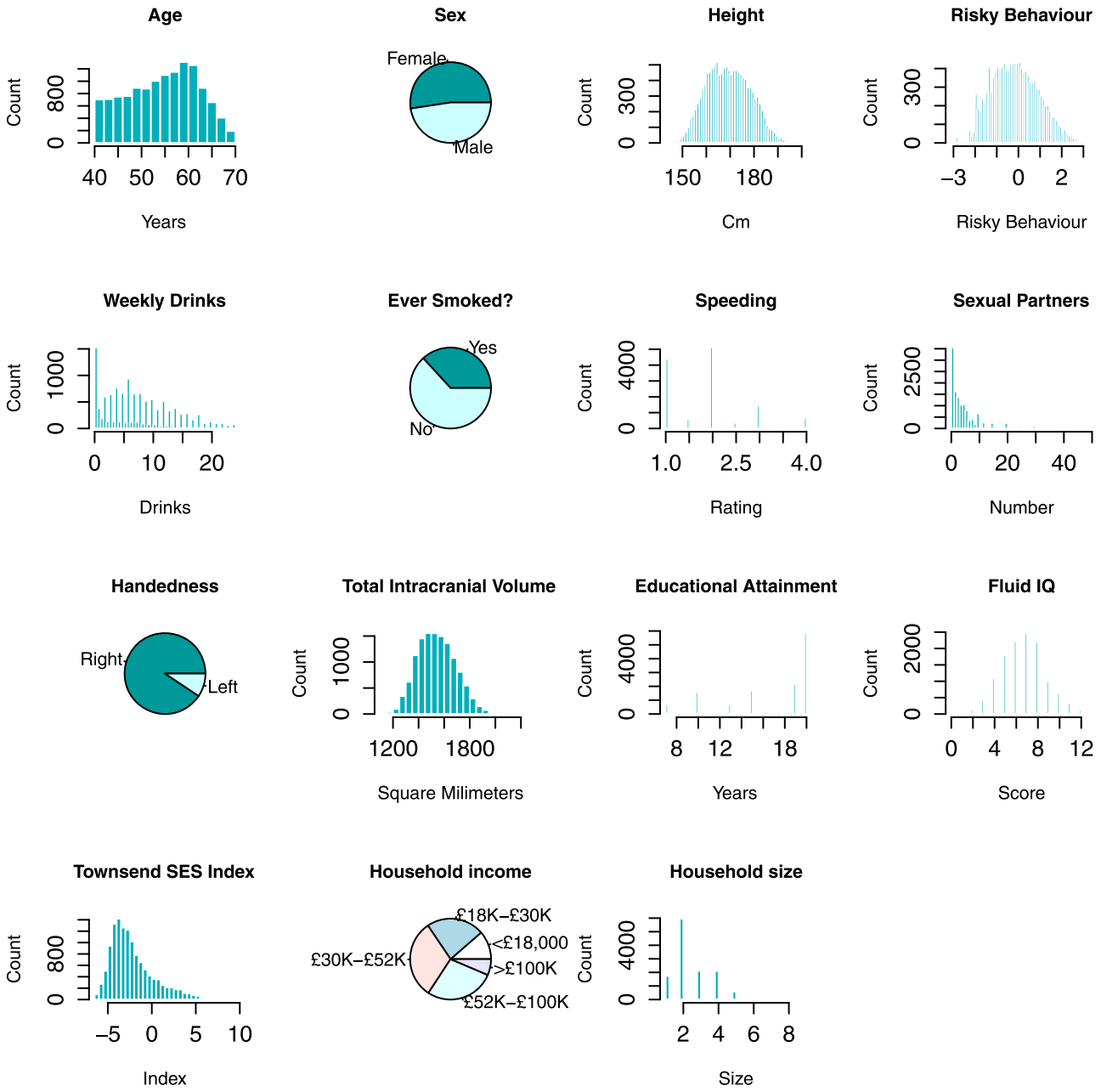

Extended Data Fig. 2 | Empirical distributions of variables in the replication sample (N = 13,004).

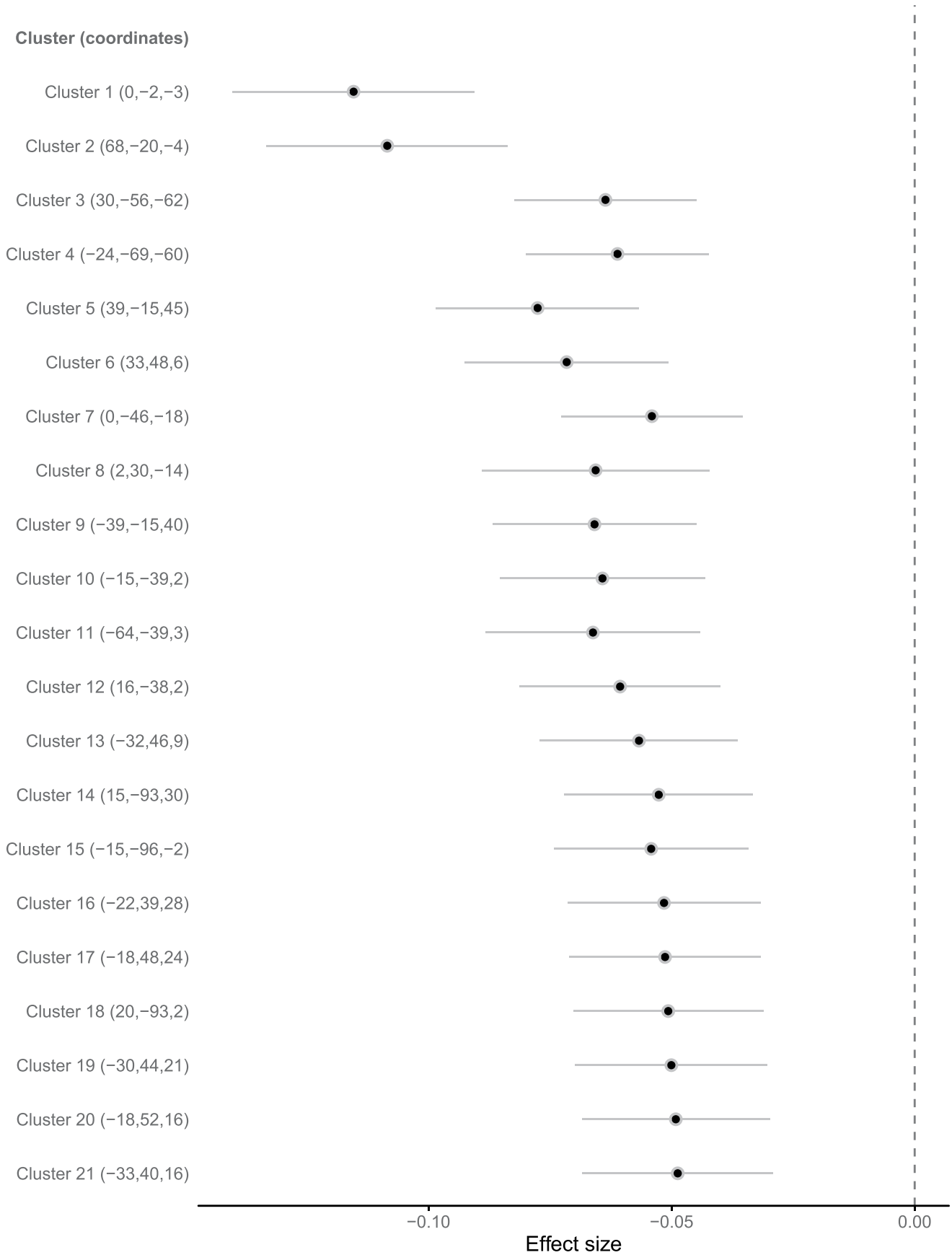

Extended Data Fig. 3 | Effect sizes (standardized betas) of associations between risky behaviour and grey matter volume (GMV) in voxel clusters showing significant associations at P < .01 (FWE-corrected) (N = 12,675). Coordinates of peak association for each cluster are reported in parentheses (in mm). Standard errors denote uncorrected 95% confidence intervals. See Extended Data Table 4 for further details.

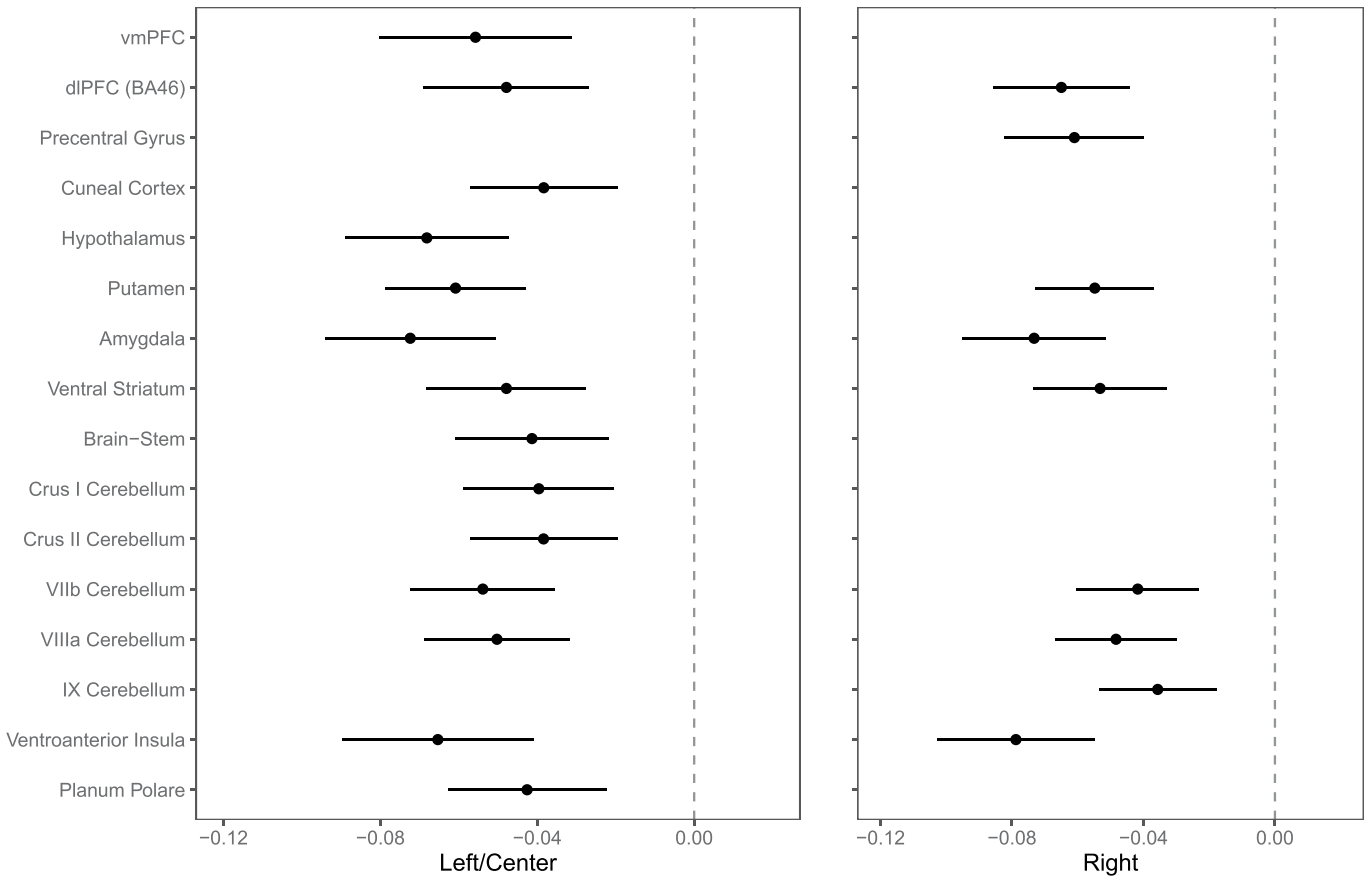

Extended Data Fig. 4 | Effect sizes (standardized betas) of association between risky behaviour and IDPs of grey matter volume (GMV) showing significant associations at P<0.01 level (FWE-corrected) (N = 12,675). Standard errors denote uncorrected 95% confidence intervals.

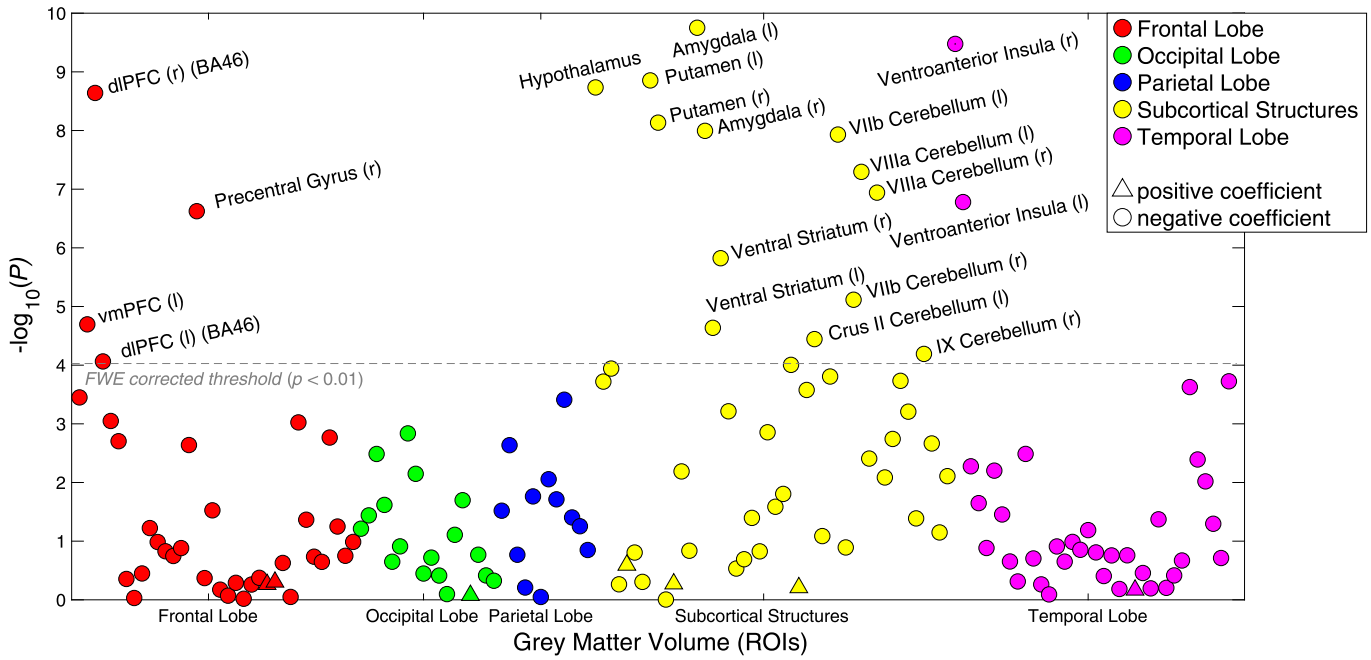

Extended Data Fig. 5 | Associations (p-values) between risky behaviour and 148 ROI-level imaging-derived phenotypes (IDPs) of grey matter volume (GMV), controlling for cognitive and socioeconomic outcomes (N = 11,864). Control variables include education years, fluid IQ, zip-code level social deprivation, household income, number of household members, birth location, and all standard controls.

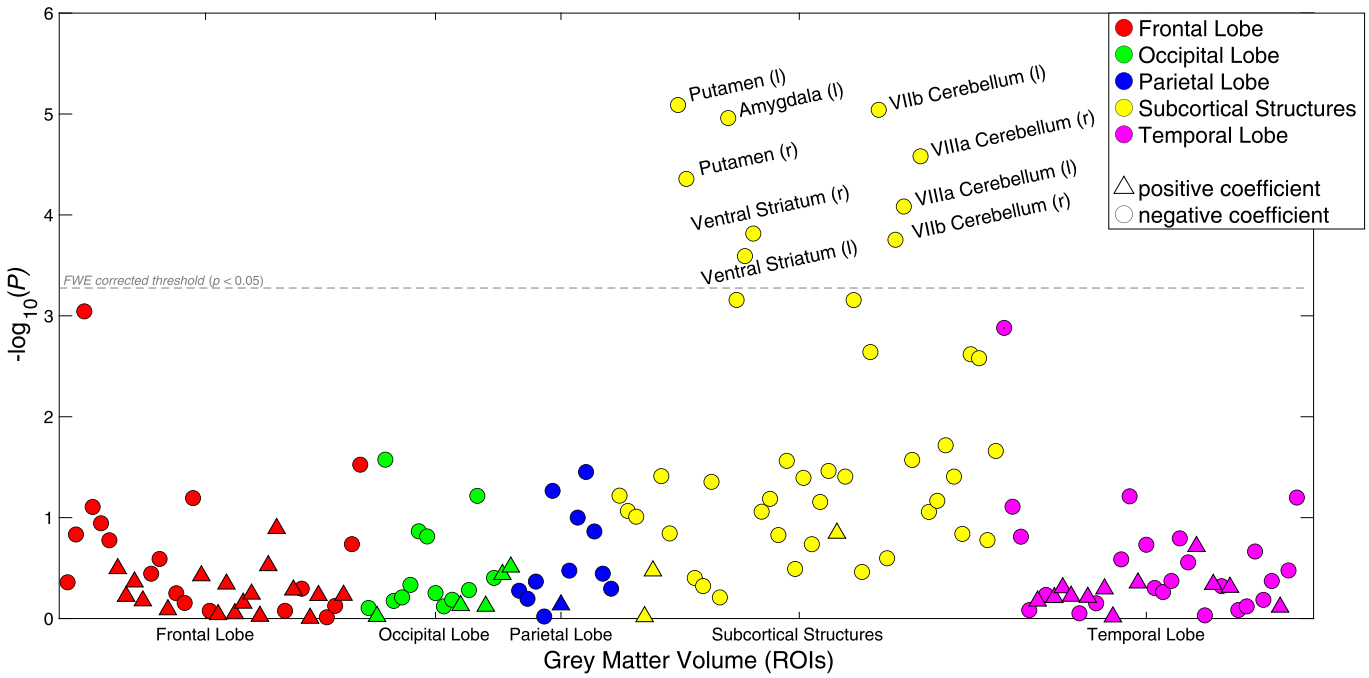

Extended Data Fig. 6 | Associations (p-values) between risky behaviour and 148 ROI-level imaging-derived phenotypes (IDPs) of grey matter volume (GMV), controlling for current drinking levels (binned in deciles) and smoking levels (binned in 3 categories) in addition to all standard controls (N = 12,675).

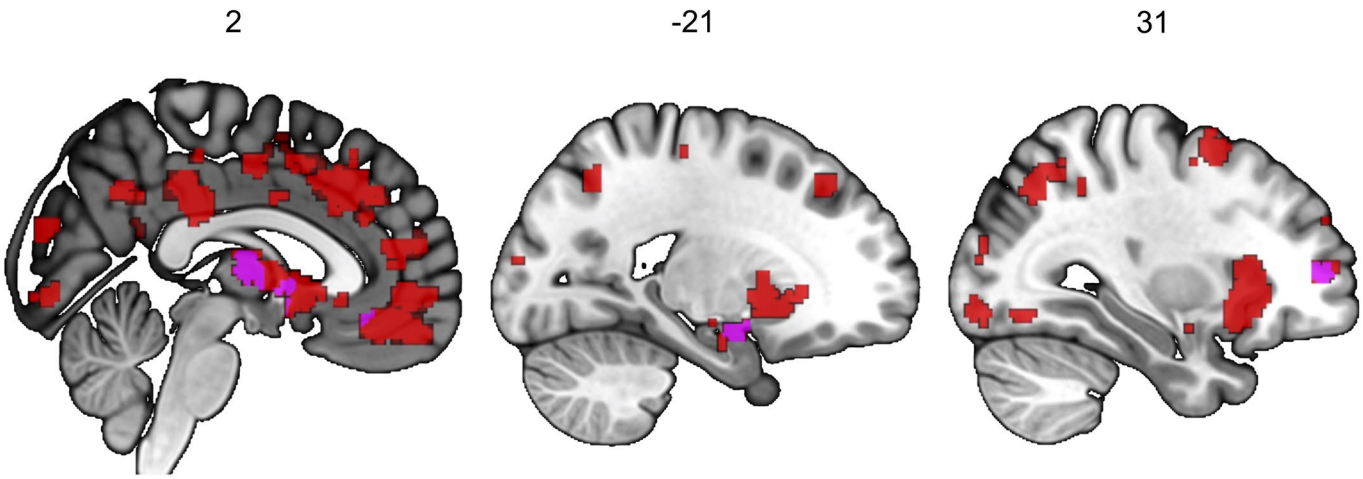

Extended Data Fig. 7 | Meta-analysis of functional MRI studies of risky behaviours, provided by Neurosynth (N = 4,717 participants and K = 101 studies). Conjunction with areas showing negative GMV association with risky behaviour (including thalamus, vmPFC, amygdala and dlPFC) is marked in magenta (see Supplementary Table 1). Additional meta-analytic functional activation areas are marked in red.

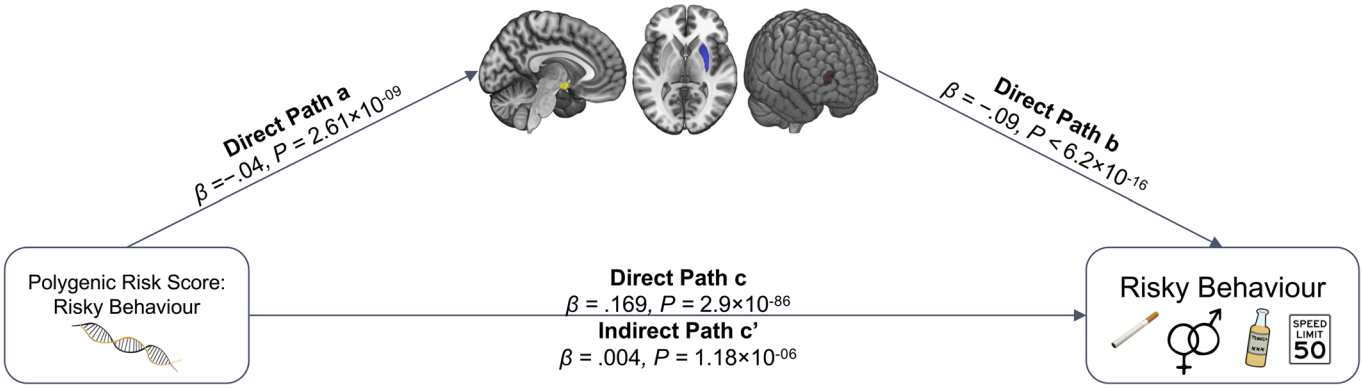

Extended Data Fig. 8 | Mediation analysis of the association between PRS and risky behaviour with GMV in dlPFC, putamen and hypothalamus (N = 12,675). The sum of all GMV differences in right dlPFC, putamen and hypothalamus (based on the activation masks from Fig 5A) mediated ~2.07% of the association between the PRS and risky behaviour. Arrows depict the direction of the structural equation modelling and do not imply causality.

nature research

Corresponding author(s): Gideon Nave

Last updated by author(s): Nov 19, 2020

Reporting Summary

Nature Research wishes to improve the reproducibility of the work that we publish. This form provides structure for consistency and transparency in reporting. For further information on Nature Research policies, see our Editorial Policies and the Editorial Policy Checklist.

Statistics

For all statistical analyses, confirm that the following items are present in the figure legend, table legend, main text, or Methods section.

n/a	Confirmed	
☐	☒	The exact sample size (*n*) for each experimental group/condition, given as a discrete number and unit of measurement
☐	☒	A statement on whether measurements were taken from distinct samples or whether the same sample was measured repeatedly
☐	☒	The statistical test(s) used AND whether they are one- or two-sided *Only common tests should be described solely by name; describe more complex techniques in the Methods section.*
☐	☒	A description of all covariates tested
☐	☒	A description of any assumptions or corrections, such as tests of normality and adjustment for multiple comparisons
☐	☒	A full description of the statistical parameters including central tendency (e.g. means) or other basic estimates (e.g. regression coefficient) AND variation (e.g. standard deviation) or associated estimates of uncertainty (e.g. confidence intervals)
☐	☒	For null hypothesis testing, the test statistic (e.g. *F*, *t*, *r*) with confidence intervals, effect sizes, degrees of freedom and *P* value noted *Give P values as exact values whenever suitable.*
☒	☐	For Bayesian analysis, information on the choice of priors and Markov chain Monte Carlo settings
☒	☐	For hierarchical and complex designs, identification of the appropriate level for tests and full reporting of outcomes
☐	☒	Estimates of effect sizes (e.g. Cohen's *d*, Pearson's *r*), indicating how they were calculated

Our web collection on statistics for biologists contains articles on many of the points above.

Software and code

Policy information about availability of computer code

Data collection	The data is publicly available to researchers upon application to the UK Biobank: https://www.ukbiobank.ac.uk/
Data analysis	Analyses code is available on the project's page on OSF: https://osf.io/qkp4g/

For manuscripts utilizing custom algorithms or software that are central to the research but not yet described in published literature, software must be made available to editors and reviewers. We strongly encourage code deposition in a community repository (e.g. GitHub). See the Nature Research guidelines for submitting code & software for further information.

Data

Policy information about availability of data

All manuscripts must include a data availability statement. This statement should provide the following information, where applicable:

- Accession codes, unique identifiers, or web links for publicly available datasets
- A list of figures that have associated raw data
- A description of any restrictions on data availability

The data is publicly available to researchers upon application to the UK Biobank: https://www.ukbiobank.ac.uk/

Field-specific reporting

Please select the one below that is the best fit for your research. If you are not sure, read the appropriate sections before making your selection.

☒ Life sciences ☐ Behavioural & social sciences ☐ Ecological, evolutionary & environmental sciences

For a reference copy of the document with all sections, see nature.com/documents/nr-reporting-summary-flat.pdf

Life sciences study design

All studies must disclose on these points even when the disclosure is negative.

Sample size	Our initial sample consisted of N = 18,796 individuals with brain scans and genotype data, all of the imaged UKB participants as of 18 Oct 2018. Our final dataset (after exclusions) consisted of N = 12,675 individuals.
Data exclusions	From the text (supplementary materials and methods/ Sample Characteristics and Selection Criteria): We excluded 923 subjects with problematic genotype data (N = 14), putative sex chromosome aneuploidy (N = 6), a mismatch between genetic and reported sex (N = 10) or non-European ancestry (N = 893). To minimize the potential influence of neurotoxic effects due to excessive alcohol intake (4), we excluded past or current heavy drinkers from the sample (531 female and 793 male participants), where heavy drinking was defined as consuming more than 24 drinks per week for males and more than 18 drinks per week for females (5). To exclude potential former drinkers, we also removed 426 participants who indicated that they don't drink alcohol. All of the structural T1 MRI images used in the study underwent automated quality control by the UKB brain imaging processing pipeline (6). We ran additional quality checks on the images using the Computational Anatomy Toolbox (CAT; www.neuro.uni-jena.de/cat/) for SPM (www.fil.ion.ucl.ac.uk/spm/software/spm12/). This resulted in the removal of additional 747 individuals who exhibited substantial image inhomogeneity (overall volume correlation below two standard deviations from the mean). Finally, we removed all participants with incomplete behavioral data of interest or control variables (N = 2,701). Our final dataset consisted of N = 12,675 individuals.
Replication	We replicate our findings in an independent sample recruited from the same population (N=13,004)
Randomization	N/A (non-experimental study)
Blinding	N/A (non-experimental study)

Reporting for specific materials, systems and methods

We require information from authors about some types of materials, experimental systems and methods used in many studies. Here, indicate whether each material, system or method listed is relevant to your study. If you are not sure if a list item applies to your research, read the appropriate section before selecting a response.

Materials & experimental systems

n/a	Involved in the study
☒	☐ Antibodies
☒	☐ Eukaryotic cell lines
☒	☐ Palaeontology and archaeology
☒	☐ Animals and other organisms
☐	☒ Human research participants
☒	☐ Clinical data
☒	☐ Dual use research of concern

Methods

n/a	Involved in the study
☒	☐ ChIP-seq
☒	☐ Flow cytometry
☐	☒ MRI-based neuroimaging

Human research participants

Policy information about studies involving human research participants

Population characteristics	We used publicly available data from the UK Biobank (UKB), which recruited 502,617 people aged 40 to 69 years from the general population across the United Kingdom.
Recruitment	Recruitment was done by the UK Biobank
Ethics oversight	All UKB participants provided written informed consent and the study was granted ethical approval by the North West Multi-Centre Ethics committee.

Note that full information on the approval of the study protocol must also be provided in the manuscript.

Magnetic resonance imaging

Experimental design

Design type	GMV and ROI analysis of T1-weighted structural brain MRI images
Design specifications	N/A
Behavioral performance measures	Self-reports

Acquisition

Imaging type(s)	T1-weighted structural brain MRI images in NIFTI format
Field strength	3T
Sequence & imaging parameters	The images were acquired using 3-T Siemens Skyra scanners, with a 32-channel head coil (Siemens, Erlangen, Germany), with the following scanning parameters: repetition time = 2000 ms; echo time = 2.1 ms; flip angle = 8°; matrix size = 256 × 256 mm; voxel size = 1 × 1 × 1 mm; number of slices = 208.
Area of acquisition	Whole brain

Diffusion MRI ☐ Used ☒ Not used

Preprocessing

Preprocessing software	We preprocessed the data using the Computational Anatomy Toolbox (CAT; www.neuro.uni-jena.de/cat/) for SPM12 (www.fil.ion.ucl.ac.uk/spm/software/spm12/). Image pre-processing used the default setting of CAT12 (accessible online at http://www.neuro.uni-jena.de/cat12/CAT12-Manual.pdf). Images were corrected for bias-field inhomogeneities, segmented into gray matter, white matter, and cerebrospinal fluid (CSF), spatially normalized to the MNI space using linear and non-linear transformations, and were modulated to preserve the total amount of signal in the original image during spatial normalization (the specific SPM-processing parameters can be found in the pre-registered document on OSF https://osf.io/qkp4g/). We applied spatial smoothing with 8-mm Full-Width-at-Half-Maximum (FWHM) Gaussian kernel for the segmented, modulated images for grey matter volume (GMV).
Normalization	We spatially normalized images to MNI152 space using linear and non-linear transformations (see CAT12 image normalization at http://www.neuro.uni-jena.de/cat12/CAT12-Manual.pdf)
Normalization template	DARTEL and Geodesic Shooting templates in MNI space (CAT12 manual): "These templates were derived from 555 healthy control subjects of the IXI-database (http://www.brain-development.org) and are available in the MNI space for six different iteration steps of the DARTEL and Geodesic Shooting normalization."
Noise and artifact removal	Denoising from the CAT12 manual: "We also use two noise reduction methods to make data processing, and the tissue segmentation in particular, more robust against noise. The first method is a spatial-adaptive Non-Local Means (SANLM) denoising filter and removes noise while maintaining edges (Manjón et al., 2010) and is implemented as pre-processing step. The second method is a classical Markov Random Field (MRF) approach, which includes spatial information from adjacent voxels in the segmentation estimation (Rajapakse et al., 1997) and is part of the AMAP segmentation. The strength of the filters is automatically determined by estimating the residual noise in the image or can be set manually."
Volume censoring	Following standard VBM procedures (see SPM/CAT12 http://www.neuro.uni-jena.de/cat12/CAT12-Manual.pdf) we thresholded the average of all brain images at 250 GMV intensity units. The resulting image was binarized and applied as a pre-mask to all individual images before running analyses. Additionally, on an individual level, we excluded all voxels that exhibited a lower grey matter volume than .1 from the analyses (see standard parameters of SPM/CAT12 http://www.neuro.uni-jena.de/cat12/CAT12-Manual.pdf).

Statistical modeling & inference

Model type and settings	Linear Regression models at the voxel or ROI level.
Effect(s) tested	N/A

Specify type of analysis: ☐ Whole brain ☐ ROI-based ☒ Both

Anatomical location(s): Whole brain

Statistic type for inference (See Eklund et al. 2016)	voxel level (or ROI level) permutation tests

Correction	FWE

Models & analysis

n/a	Involved in the study
☒	☐ Functional and/or effective connectivity
☒	☐ Graph analysis
☒	☐ Multivariate modeling or predictive analysis